metals

MDPI

Article

On the Use of Functionally Graded Materials to Differentiate the Effects of Surface Severe Plastic Deformation, Roughness and Chemical Composition on Cell Proliferation

Laurent Weiss [1,2,*], Yaël Nessler [2], Marc Novelli [1], Pascal Laheurte [1,2] and Thierry Grosdidier [1,2]

[1] Laboratoire d'Etude des Microstructures et de Mécanique des Matériaux, Université de Lorraine, 57073 Metz, France; Marc.novelli@univ-lorraine.fr (M.N.); pascal.laheurte@univ-lorraine.fr (P.L.); thierry.grosdidier@univ-lorraine.fr (T.G.)

[2] Laboratory of Excellence for Design of Alloy Metals for Low-Mass Structures ('DAMAS' Labex), Université de Lorraine, 57070 Metz, France; nessler.yael@hotmail.fr

* Correspondence: Laurent.weiss@univ-lorraine.fr; Tel.: +33-3-72-74-77-87

Received: 20 November 2019; Accepted: 6 December 2019; Published: 13 December 2019

Abstract: Additive manufacturing allows the manufacture of parts made of functionally graded materials (FGM) with a chemical gradient. This research work underlines that the use of FGM makes it possible to study mechanical, microstructural or biological characteristics while minimizing the number of required samples. The application of severe plastic deformation (SPD) by surface mechanical attrition treatment (SMAT) on FGM brings new insights on a major question in this field: which is the most important parameter between roughness, chemistry and microstructure modification on biocompatibility? Our study demonstrates that roughness has a large impact on adhesion while microstructure refinement plays a key role during the early stage of proliferation. After several days, chemistry is the main parameter that holds sway in the proliferation stage. With this respect, we also show that niobium has a much better biocompatibility than molybdenum when alloyed with titanium.

Keywords: surface mechanical attrition treatment (SMAT); ultrasonic shot peening (USP); functionally graded materials (FGM); titanium niobium alloys; titanium molybdenum alloys; human mesenchymal stem cells culture; cell adhesion; cell proliferation

1. Introduction

Improving the biocompatibility of titanium and titanium alloy prostheses is a major challenge for the biomedical industry and has been the subject of much scientific interest in recent years [1,2]. Among all the techniques allowing the improvement of the cells adhesion and proliferation, severe plastic deformation (SPD) of the material has been studied for about one decade and, since then, been the subject of several investigations. SPD makes it possible to refine the microstructure to obtain, under some specific conditions, a nanostructure. The first biocompatibility study on pure titanium deformed by SPD was carried out by Kim et al. in 2007 [3]. The results have shown that the refinement of the microstructure by equal-channel angular pressing (ECAP) leads to a better wettability and therefore a better adhesion and proliferation of fibroblasts after two and five days. In a second study, the same research group has shown that the cytotoxicity remained unchanged after SPD [4]. Other teams have shown that ECAP also leads to a better proliferation of mouse fibroblasts after 72 h [5] and a better adhesion of human mesenchymal stem cells (MSCs) [6]. Further, other investigations have shown that ECAP can be followed by chemical etching or sanding to create surface pores that further increase the

bio-integration [7,8]. The high pressure torsion (HPT) [9] is another technique of grain refinement by core SPD that can improve the biocompatibility as illustrated on NiTi [10] alloys as well as on pure titanium by modification of its protective oxide layer [11]. This modification of the oxide layer on Ti-based materials has recently been demonstrated by other teams using other SPD techniques [12–14]. These positive results on the effect of core SPD have nonetheless been counterbalanced by some studies which have shown no beneficial effect of SPD or equivalent results for coarse-grain and nano-grain microstructures [15,16].

These core SPD techniques impart the plastic deformation to the overall material while, in many cases, only the surface is an important issue in terms of bio-integration. Thus, an interesting prospect for bio-integration is to modify the surface properties while preserving at core the mechanical properties of the raw material. With this respect, techniques have been applied to create surface graded microstructures by surface SPD such as, for example, sliding friction treatment (SFT) [17] as well as surface mechanical attrition treatment (SMAT) [18]. The first one has shown promising results in terms of biocompatibility [13] but remains very difficult to implement industrially. The SMAT technique, also called ultrasonic shot peening (USSP), is already used in industry to increase the fatigue resistance of prosthesis [19] and has already proven its ability to increase the biocompatibility of titanium alloys. SMAT consists of plastically deforming the sample surface by moving shots set in motion by an ultrasonic vibrating part called sonotrode. The main difference compared to conventional directional peening is that, in the case of SMAT, the shots are moving within a sealed chamber giving them random impact trajectories on the surface, enhancing the superficial structural refinement [18,20]. A complete description of the treatment can be found in [21]. This treatment results in nanostructuring of the material but also in an increase in the surface roughness [18,20,21] and, apparently, an increase in surface wettability [22]. Results on pure titanium have revealed an increase in adhesion and viability of MSCs [23]. In-vivo tests on rabbits have been done to compare SMATed and raw Ti6Al4V and the study showed better bio-integration of the surface SPD materials within the bones after four, eight and 12 weeks [24].

The results on bio-integration by SPD nevertheless raise an important question: to greatly improve the biocompatibility, is it better to change the roughness, the size of the microstructure or the chemistry of the material? To answer this question, the latest advances in additive manufacturing that allow to manufacture parts made of functionally graded material (FGM) are here tested in combination with SMAT to ensure that all preparations have been made., Following this, the cell cultures are made under exactly the same atmosphere and in the same environment (temperature, time).

These types of materials, born in the 1980s in Japan [25], can be classified into three distinct groups depending on the nature of the gradients: gradient in microstructure, gradient in porosity and gradient in composition. In the present work, gradients in composition (Ti-Nb and Ti-Mo) will be tested. The functionally graded composition is defined by Pei et al. as "a change in composition across the bulk volume of a material aimed to dynamically mix and vary the ratios of materials within a three dimensional volume to produce a seamless integration of monolithic functional structures with varied properties" [26]. FGM are already used to provide an enhanced substitute for the coating in orthopedic implants, thus avoiding the sudden change in chemical composition and the "peeling-off" effect of the coated [27]. Several advantages can be achieved, such as improving the fixation of implant to bone, enhancing the stress shielding phenomena, hardening the articulating surface, and removing interfacial stresses between the implant and bone.

Bogdanski et al. were the first to use a FGM metal (Ni-Ti) ranging from 0 to 100% to find the composition with the best biocompatibility [28]. Unfortunately, the combination of cold isostating pressing (CIP) + hot isostating pressure (HIP) + vacuum welding processes used at this time was both time-consuming and costly.

Nowadays, direct energy deposition (DED) makes it possible to manufacture FGMs more rapidly and at a lower cost with two or more materials. This additive manufacturing technique, that uses a powder spray, has been successfully tested on FGM titanium-based alloys [29,30]. Since it can be

used to manufacture prostheses with surface properties that are different from those of the core, these FGMs have a strong potential for the future in the biomedical industry [31]. Among all material couples, titanium-niobium alloys and titanium-molybdenum alloys are excellent candidates for new prostheses generation [32,33]. In this interest, the aim of this study is thus to investigate the effect of chemistry, roughness and SMATed microstructure on cell adhesion and proliferation. To this end, FGMs have been made based on the Ti-Nb and Ti6Al4V-Mo constituents and then treated by SMAT. The FGMs compositions range from 100% Ti to 100% Nb as well as 100% Ti6Al4V to 100% Mo and were manufactured with a DED technique called CLAD® [34,35]. The FGMs were investigated in their polished (P), SMATed (S) and SMATed + polished (S+P) conditions then human mesenchymal stem cells were deposited and counted as function of time from three up to 21 days.

2. Experimental Procedure

2.1. Sample Preparation

The samples were manufactured at Irepa Laser using a CLAD®machine (Magic 800, BEAM company, Strasbourg, France) under a neutral argon atmosphere using a Ti6Al4V support plate. In this technology, the powder is injected into a laser beam and melts before falling onto the substrate. The machine can be fed simultaneously by different powder feeders, so it becomes possible to real-time control the chemical composition of the powder mixture. The size distribution of the powder particles measured by laser diffraction analysis is given in Table 1. As sketched in Figure 1, the manufactured gradient materials contain respectively 0, 25, 50, 75 and 100% of Nb or Mo and, conversely, 100, 75, 50, 25 and 0% of Ti or Ti6Al4V. The size of the parts is also given in Figure 1a. The powders and manufacturing data (power, speed, pitch, etc.) of the samples have been detailed in the works of Schneider et al. [34,35].

Table 1. Size distribution of the different powders in μm [34,35].

Material	D_{10}	D_{50}	D_{90}
Ti	54	73	100
Nb	41	56	76
Ti6Al4V	58	80	109
Mo	45	61	82

The FGM walls were cut into 1.5 mm thick slices. To take into account the effects of the surface roughness, the samples have been divided into three categories: polished (P), SMATed (S) and SMATed then polished (S + P). The P samples were polished using OPS (Oxide Polishing Suspension, Struers, Champigny-sur-Marne, France) to obtain a mirror-like surface. Samples S and S + P were SMATed for 5 min (frequency 20 kHz, amplitude 60 microns) with 2 mm spherical shots made of 100C6 steel. The shot blasting time was deliberately chosen to be short enough to minimize any possible transfer of chemical species coming from the shot-balls or tooling that are known to pollute the surface under SMAT [21,36–40]. This type of pollution, which is known to develop for long term peening, has been demonstrated to affect the corrosion properties of some parts [39,40] can indeed also have an effect on biological tests. After SMAT, the S + P samples were polished with OP-S over 2 or 3 μm to modify the roughness issued from the SMAT process while remaining in the area where the microstructure was modified. This experimental procedure using FGMs coupled with surface SPD as well as polishing has several advantages. While the comparison between the S and S + P samples makes it possible to study the effect of the roughness created by the SMAT for a given type of refined structure, the comparison between the P and S + P samples authorizes to analyze the effect of the microstructure modification by SPD for a mirror-like surface. In addition, the comparison of the response along the same sample can

be used to depict the effect of the chemistry as well as the comparison between Ti-Nb and Ti6Al4V-Mo can be used to find the most biocompatible alloying element.

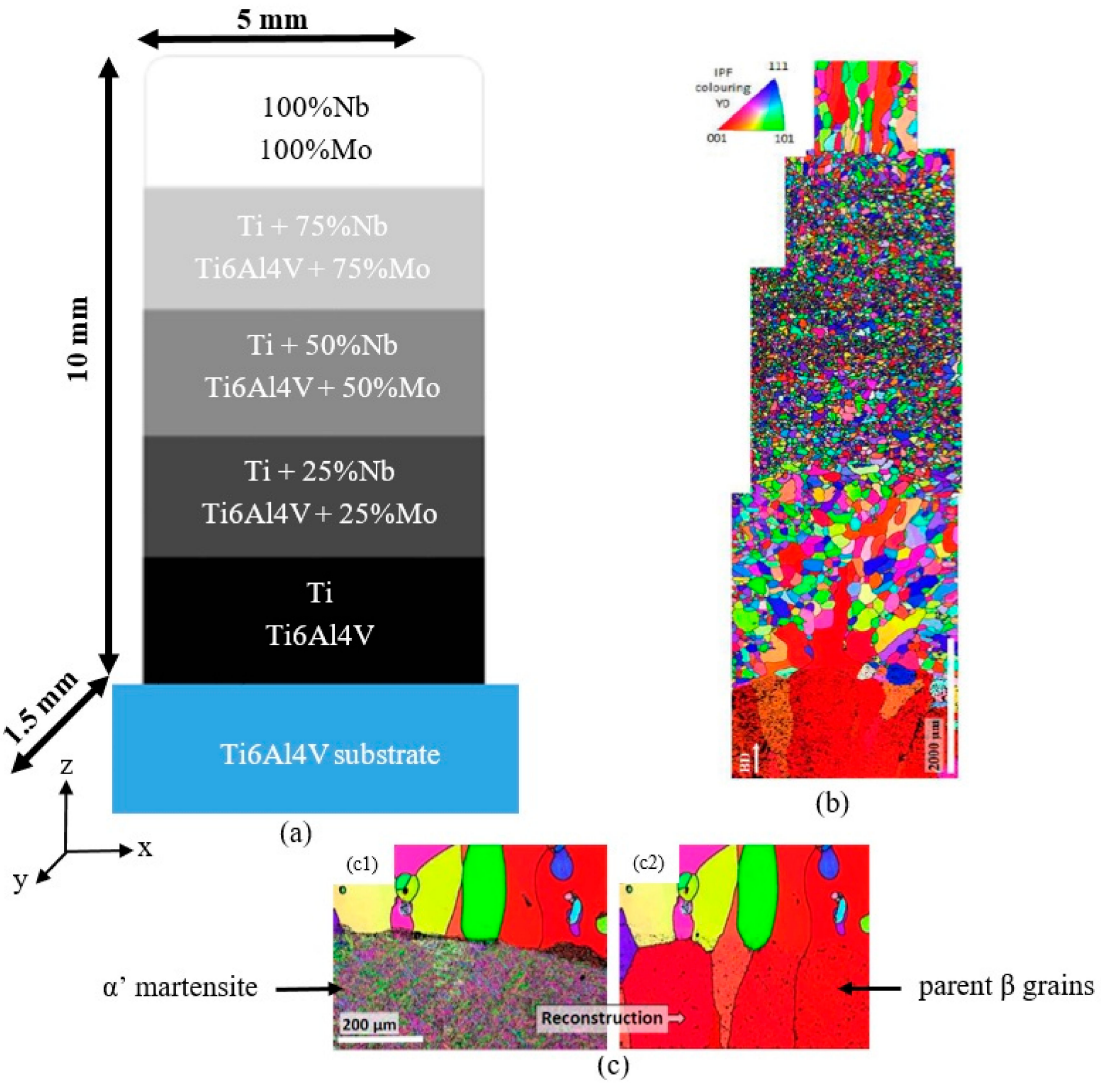

Figure 1. (**a**) Size and chemical composition of the samples for the Ti/Nb and Ti6Al4V/Mo couples; (**b**) complete map of the Ti6Al4V-Mo FGM after reconstruction from Schneider et al. [35]; (**c**) example of the interface Ti6Al4V/Ti6Al4V + 25% Mo before (**c1**) and after beta reconstruction (**c2**).

2.2. Roughness and Microscopy

The roughness measurements were carried out with a focus-variation microscopy using an Alicona Infinite Focus apparatus. The values presented are the average of 200 lines of 400 µm long. The microstructure of the samples was analyzed on the cross-section after OPS polishing with a Supra40 Scanning Electron Microscope (Carl Zeiss, Oberkochen, Germany).

2.3. Sterilization and Cell Culture

The samples were first placed in 12-well plates and then immersed in 1 mL of ethanol for 30 min. The plates were then placed in a sterile hood where they were exposed to UV for 30 min. To ensure perfect sterilization, the samples were then cleaned with bleach and then autoclaved for 4 h at 120 °C.

For each sample (P, S and S + P), the tests were performed three times with MSCs from three different donors. The cells were thawed one week before seeding and all manipulations were performed under hood using sterile equipment. The inoculated samples were placed in an incubator at 37 °C, 5%

CO_2 and 90% humidity. After 45 min, 1 mL of α MEM (Minimum Essential Medium) was added per well and the plates were put back into the incubator. The culture medium was changed twice a week.

The viability of the cells was checked after 3, 7, 14 and 21 days. For this, an Alamar Blue test (a resazurin blue colored indicator which transforms into pink resorufin thanks to the reducing power of mitochondria) was used. The percent difference in reduction is proportional to the metabolic activity of the cells, and, thus, to their viability. The tests were done in a dark sterile hood and the color change was detected using a spectrometer.

2.4. Cell Adhesion and Cell Counting

Paraformaldehyde was intended to freeze the cell structures in a state as close as possible to their living state. For each configuration and donor, the cells of three samples of each pair of material were fixed at 3, 7, 14 and 21 days after the start of the cell culture. The samples were placed in a new 12-well plate and then 1 mL of 4% paraformaldehyde (PAF) was added in each. The PAF acted for 10 min, then it was removed and the samples were washed with phosphate buffered saline (PBS).

A 0.1% solution of 4′, 6-diamidino-2-phenylindole (DAPI), i.e., 1 µL of DAPI per 999 µL of PBS, was deposited in each well. The DAPI inserted into the DNA of the nucleus cells and emitted a 455 nm blue light when excited by 345 nm light. This allowed us to observe the cells under a fluorescence optical microscope and to count them on each section of the chemical gradient.

3. Results and Discussion

3.1. Evolution of the Microstructure Along the Gradient

The microstructure features of the different graded materials in their as-deposited states has been detailed previously [34,35]. The main features are just recalled in Figure 1b,c for the sake of clarity. The evolution of the microstructure, and in particular the parent grain morphologies after a reconstruction from the martensitic ′ variants, is illustrated in Figure 1b,c. The evolution of the microstructure for the Ti-Nb and TA64-Mo walls shared a number of aspects and the features shown in Figure 1b,c for TA64-Mo pertain for the other FGM sample. Because of the fast cooling rate [34,35], the initial layers of Ti or Ti6Al4V were characterized respectively by a Widmanstätten or a martensitic α′ microstructure, issued from the high temperature parent phase nucleated from the melt (Figure 1c). With the addition of Nb or Mo, the microstructure became beta equiaxed with a decreasing grain size as the alloying element amount increased (Figure 1b). In the pure Niobium (Nb) or pure Molybdenum (Mo) layers, the beta grains were columnar parallel to the z axis (deposition axis).

Figures 2 and 3 give SEM images showing details of the microstructures after the application of the SMAT process. In Ti and Ti6Al4V as well as at the lowest amount of additions (25% of Mo), the top surface microstructure was refined over a depth of the order of 5 to 15 µm. This is particularly visible in Figure 3a,b where the grains are refined and equiaxed near the surface while elongated grains are visible at the sub-surface. In addition, for the initial structure, kink bands appeared in the subsurface over significant thicknesses (>200 µm). This type of kink band has already been observed in highly alloyed beta titanium alloys during deformation at high speed rate [41]. The width of the zone where these kink bands were present was thicker for the case of the Nb addition than for the Mo one (Figures 2b and 3b). Indeed, the kink bands reached the surface for the Ti-25Nb alloy, whereas for the Ti6Al4V-25Mo alloy, the nanostructured layer was present from the surface towards 15 µm below the surface (Figure 3b). From 50% of alloying elements, the kink bands disappeared and the contrast visible within the beta grains at the SMATed surface witnessed strong internal misorientations. Figures 2c–e and 3c–e show that the thickness of this layer depends on the amount in alloying element. A comparison of the blue and red arrows in Figures 2c–e and 3c–e indicates, however, that its thickness is equivalent for both the Ti-Nb and Ti6Al4V-Mo alloys at a given amount of alloying element.

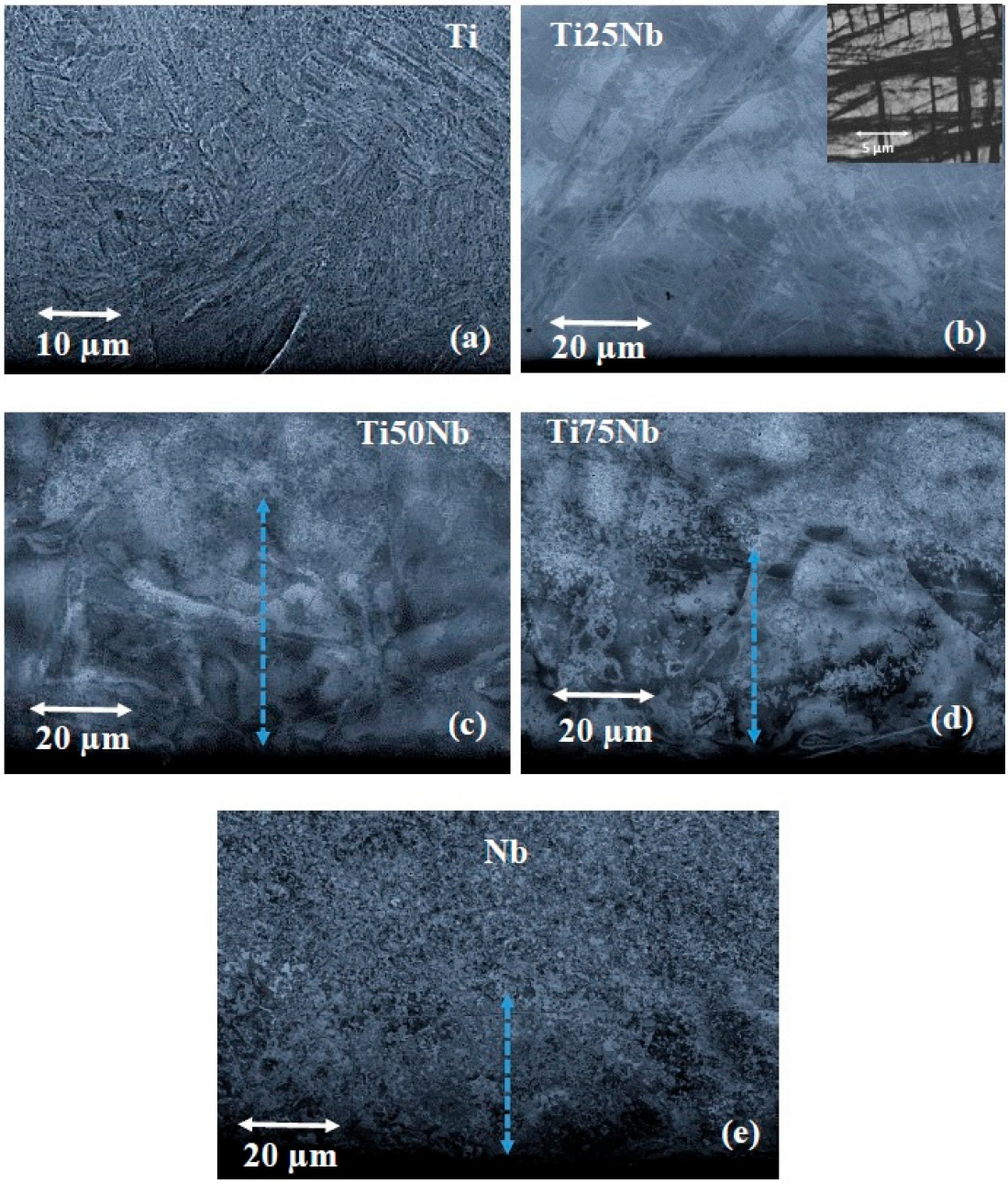

Figure 2. (**a**–**e**): cross section pictures of the surface mechanical attrition treatment (SMAT)ed TiNb sample focused on the severe plastic deformed region (the SMATed edges are always at the bottom of the pictures); (**b**): in the top right corner, focus on the kink bands at 20 µm from the surface in the Ti-25Nb; (**c**–**e**): the blue arrow represents the affected depth.

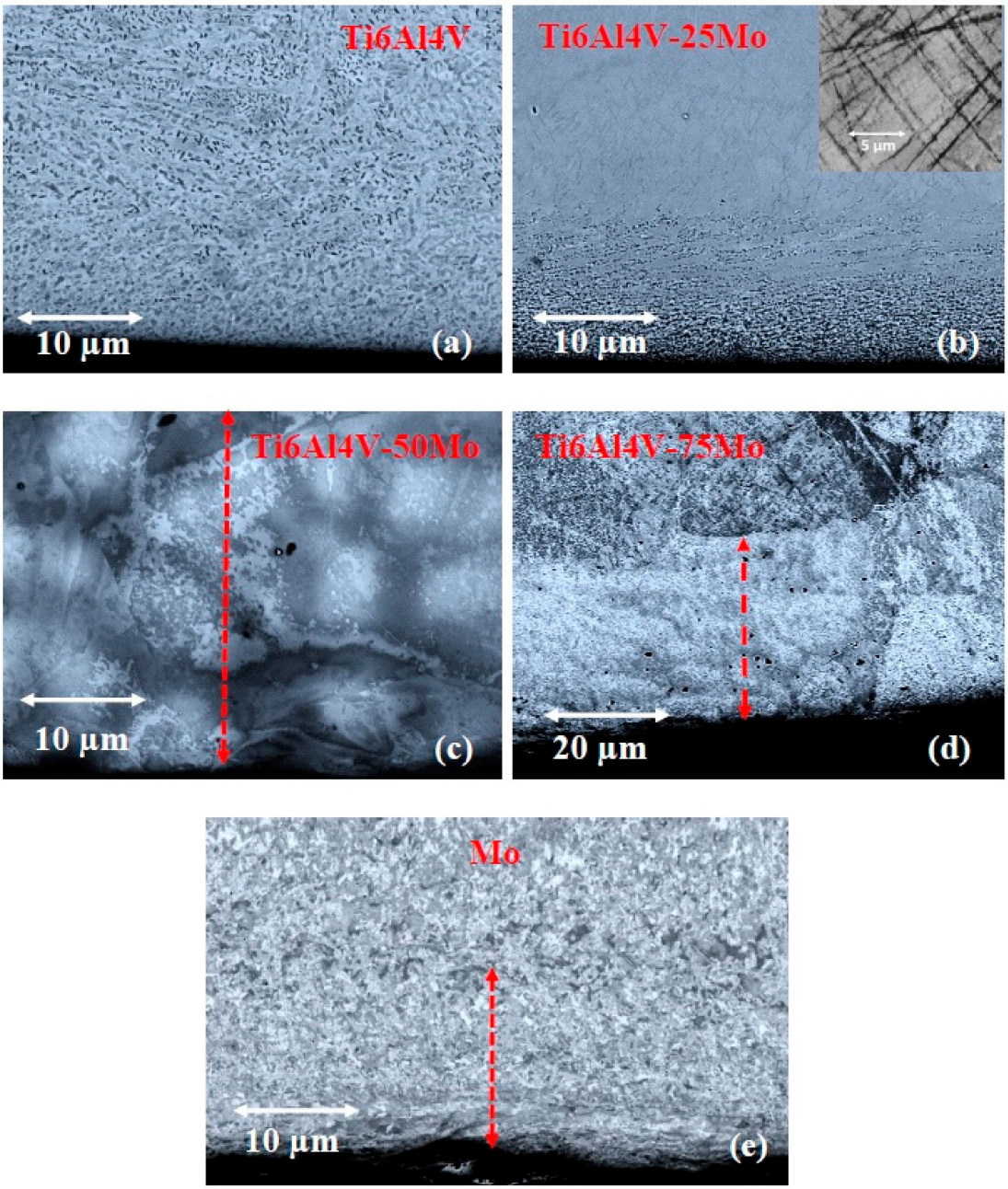

Figure 3. (**a**–**e**): Cross section pictures of the SMATed TiMo sample focused on the severe plastic deformed region (the SMATed edges are always at the bottom of the pictures); (**b**): in the top right corner, focus on the kink bands at 20 µm from the surface in the Ti6Al4V-25Mo; (**c**–**e**): the red arrow represents the affected depth.

3.2. Hardness and Roughness Evolutions

Figure 4 shows the evolution of the hardness and roughness before and after the different SMAT and SMAT + polishing treatments for the Ti-Nb wall. For the polished sample, the maximum hardness was reached for 25% of Nb (Figure 4a). According to the literature [42,43], this increase is due to the presence of a small fraction of ω-phase, especially when the composition is around 25% Nb. The amount of omega phase was increased by the successive remelting and tempering from the successive layer by layer deposition generated by the DED-CLAD process. This tempering promoted the formation of the ω-phase, which explains the increase in the microhardness, as was also observed for TiMo alloys [44].

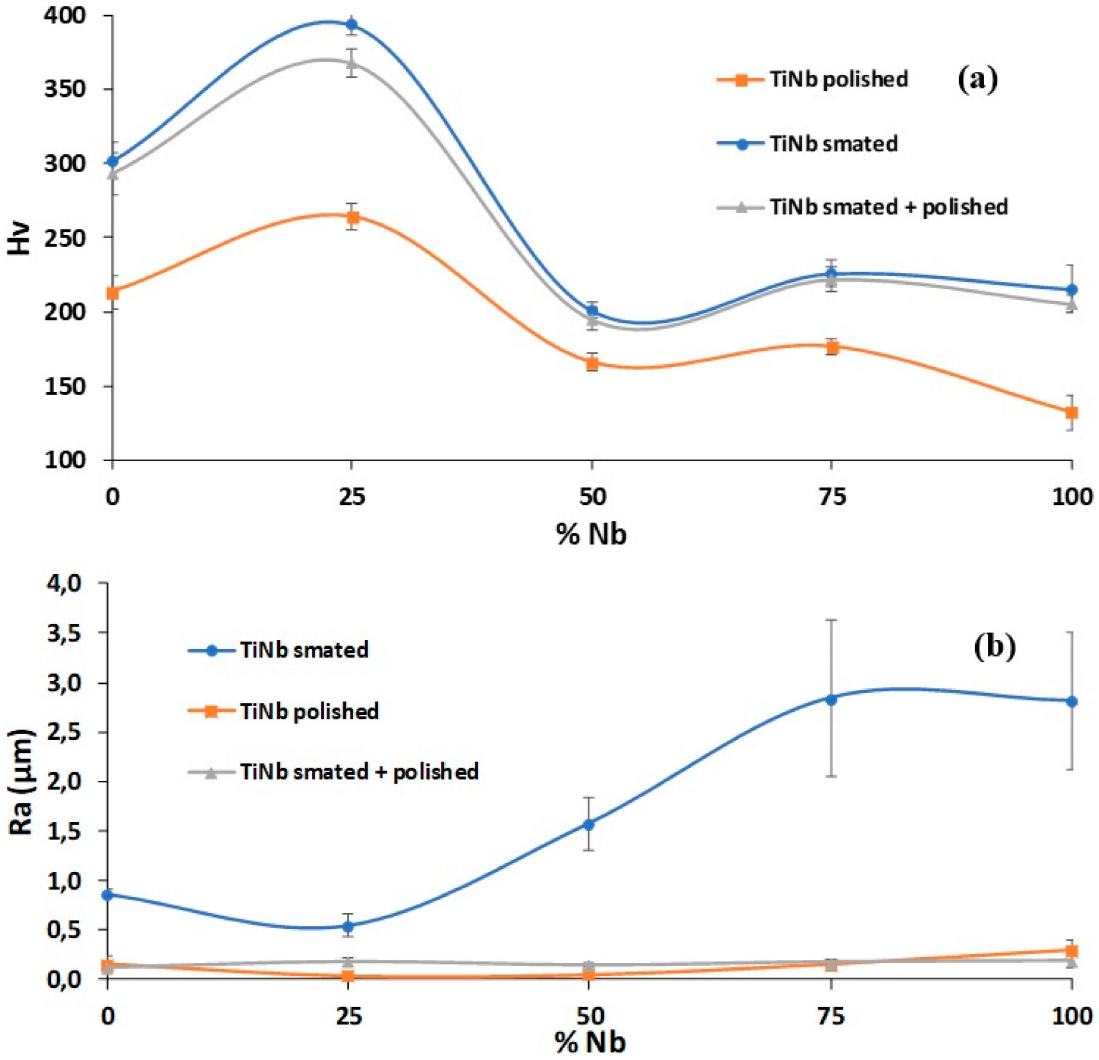

Figure 4. Evolution of (**a**) the hardness ($HV_{0.3}$) and (**b**) the roughness (Ra) as a function of the Nb alloying amount for the P, S and P + S conditions of the TiNb walls.

After the SMAT modifications, it was first interesting to notice that the hardness evolutions for the S and S + P samples are almost equal (Figure 4a). This meant that the polishing has allowed to remove a few microns to smooth the roughness (Figure 4b) while remaining in the hyperdeformed thickness. The range of hardness increase by shot peening depended slightly on the alloying amount. The maximum increase was obtained due to the appearance of the kink bands in the Ti25Nb, which made it possible to change hardness from 250 to 400 Hv (60% increase). Sadeghpour et al. [45] have recently shown that there is a relation between the presence of omega phase and the formation of kink bands due to the accumulation of simple dislocation and dislocation channels, which correlates with our study. The strong internal misorientation of the 50 to 100% Nb containing samples also increased the hardness but to a lesser extent (15 to 40% increase).

The evolutions of roughness presented in Figure 4b shows that the roughness after SMAT was inversely related to the hardness. When the material was hard, the roughness increase remained moderate. This is because—for a given impact energy—the balls created deeper craters when the material was softer (Figure 4a). Because of the polishing procedure, the P and S + P samples have the same low roughness, independently of the initial hardness. These modifications of hardness versus roughness made it possible to dissociate the effect of the roughness from the other effects (chemistry and SPD induced by SMAT). Indeed, several papers have suggested that the surface roughness plays a major role in cell biology: the higher the roughness, the higher the cell adhesion [46–48].

3.3. Cell Adhesion and Cell Proliferation

3.3.1. Comparison of the Effect of Nb and Mo on Titanium Biocompatibility

Figure 5 shows the number of cells on each gradient after three and seven days for the same donor (other donors generating the same trends). This allowed us to rapidly compare the effects of chemistry, roughness and hyperdeformation. Figure 5a shows that pure titanium and Ti6Al4V have the same trends on adhesion and proliferation after three and seven days. Ti6Al4V appeared to have a slightly more beneficial effect than pure titanium on adhesion. The number of cells on polished samples after seven days remained almost unchanged which confirms the results obtained by Johansson et al. [49]. The S + P samples for both materials had the same behavior as the polished ones. The Ti SMATed samples were unlike the Ti6Al4V SMATed samples which had a sharp decrease in the number of cells after seven days. Nevertheless, whatever the material, the SMAT had a positive effect on the adhesion because of the increase of the roughness, which is consistent with previous studies from the literature [46–48]. Figure 5b shows that the biocompatibility of these two materials does not seem to be affected by the presence of low amount of alloying elements (≤25%).

When the percentage of alloying element is increased (50 and 75%), the behavior of the cells was strongly modified. Niobium was found to have an excellent biocompatibility, which greatly increased the proliferation of the cells (Figure 5c). This effect of the chemistry was more important after seven days if the samples were SMATed. This is because of the increase in the number of adhering cells, which further increased subsequently after seven days, due to the cell division process in an excellent biocompatible environment. As shown in Figure 5d, the harmfulness of molybdenum began to have a very important effect from 75%. Even for the polished sample where the adhesion was best after three days, the cells then died quickly avec seven days. The toxicity of this alloy was even greatly increased by the microstructure modification induced by the SMAT. Indeed, on the samples, S and S + P, no cell survived after seven days. These results validated the differences in biocompatibility between Nb and Mo observed by Eisenbarth et al. [50].

In the case of pure elements, as no cells adhered or survived for all conditions of pure Mo, Figure 5e demonstrates the toxicity of pure Mo and the better biocompatibility of Nb.

All these results mainly demonstrated that the best biocompatibility was obtained for the SMATed TiNb alloys when the concentration in niobium was between 50 and 75%. In addition, it was clear that SMAT has a beneficial effect only during the adhesion stage by increasing the roughness and that the toxicity of molybdenum was increased by the microstructure modification induced by SMAT.

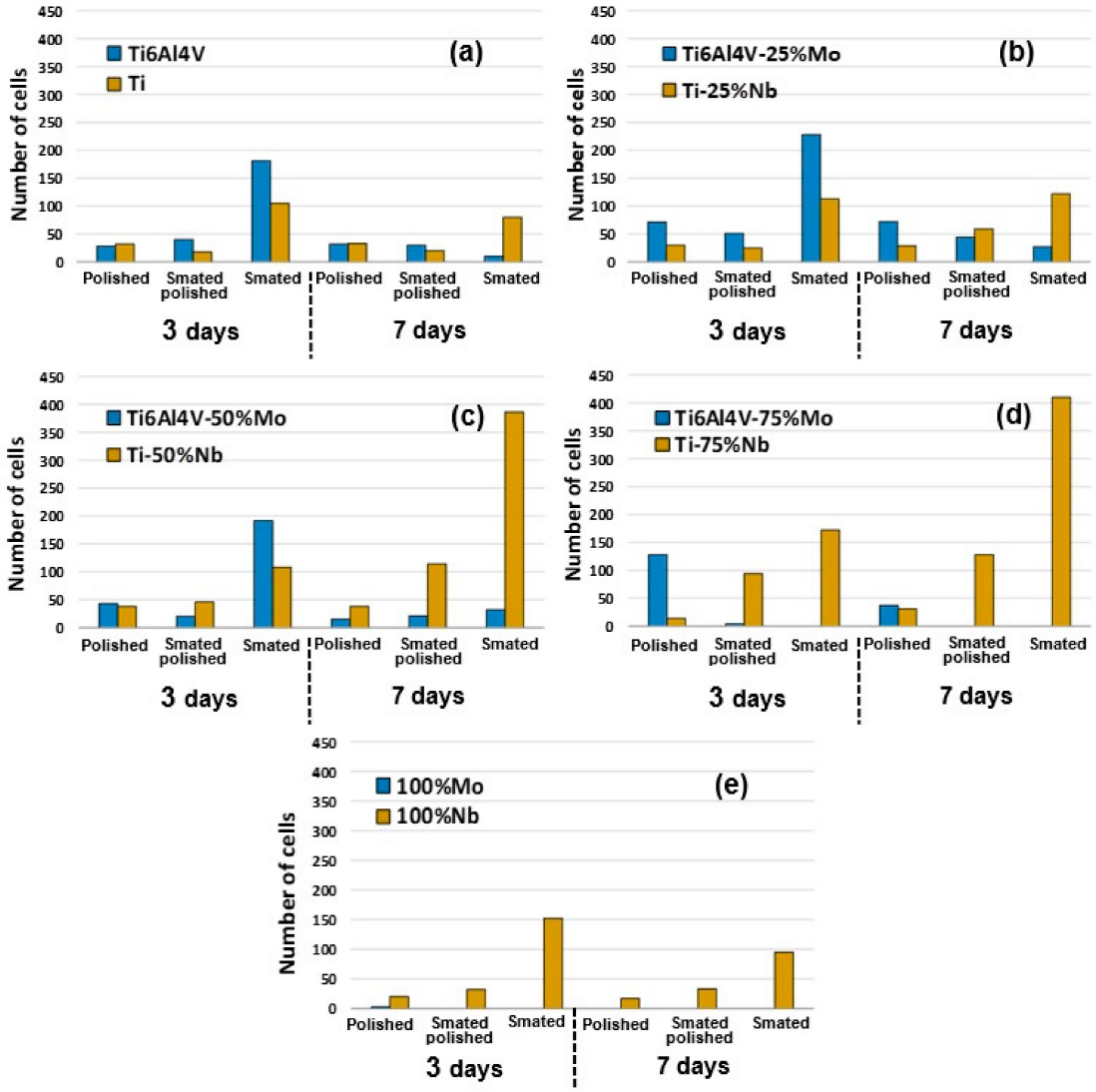

Figure 5. Comparison of the effect of Nb and Mo on cells adhesion and subsequent proliferation for different amount of alloying element. (**a**) 0%; (**b**) 25%; (**c**) 50%; (**d**) 75%; (**e**) 100%.

As the molybdenum has a poor biocompatibility compare to niobium, only the results on TiNb are showed in the rest of this paper.

3.3.2. Cell Adhesion

Figure 6 shows the average cell distributions of three donors after three and seven days. Because of the differences on the cells quality and viability between donors, the total number of healthy cells varied and it was better to calculate, for each gradient, the distribution in terms of percentages.

The comparison between Figures 4b and 6 demonstrates that, for the SMATed samples, the adhesion was preferentially done in the gradients where the roughness was important (75 and 100% of Nb). For the same roughness (P and S + P samples), the cells seemed to be randomly distributed. After seven days, the distribution trended to be the same for all samples but the nanostructured microstructure decreased the time needed to reach the distribution equilibrium. This indicated that the microstructure modification (dislocations cells, finer grains, etc.) induced by severe plastic deformation only played a role just after adhesion, at the early stage of proliferation.

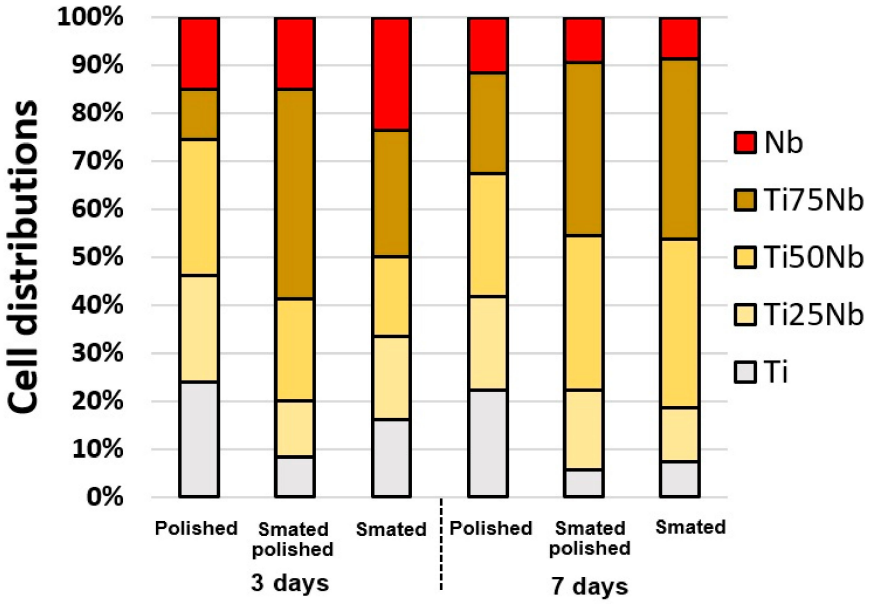

Figure 6. Cells distribution on TiNb after three and seven days.

3.3.3. Long Term Cell Proliferation on FGM

As demonstrated in Figure 5, the cells could not proliferate for the Mo containing sample and even not adhere at high Mo concentration, so only the Nb containing sample were investigated in term of cell proliferation. Figure 7 presents an example of the number of cells after three, seven, 14 and 21 days in the polished TiNb sample for the same donor. Figure 7 shows that if the total number of cells increased during the 21 days, the proliferation depended on the composition. Niobium had the fewest cells in the first week but then became the location in the gradient where proliferation was the most important. Thus, after three weeks, it became the best material with the highest cell number. Despite the fact that niobium was not used as such in prostheses because of its mechanical properties that were too far from those of the bones (higher Young modulus) [51], this test demonstrated the perfect biocompatibility of pure niobium [50]. In addition, this type of test validated the fact that FGM can be used successfully in biocompatible experiments to decrease the number of needed samples for long term proliferation test.

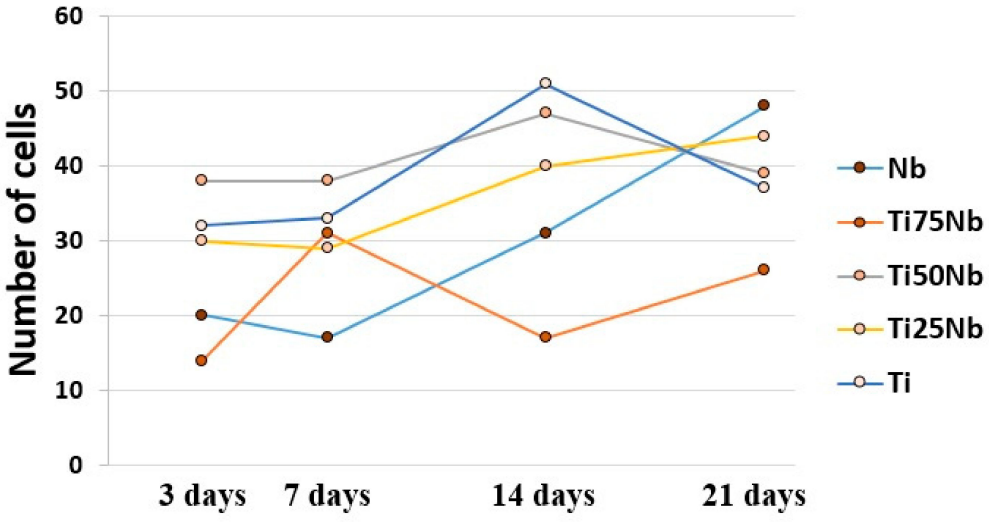

Figure 7. Cells proliferation: example of polished TiNb.

4. Conclusions

The aim of this study was to describe separately, with a single test, the effect of chemistry, roughness and SPD microstructure on MSC cell adhesion and proliferation using SMAT on two binary FGMs (Ti-Nb and TA64-Mo).

- The major findings can be summarized has follows:
- The use of FGMs can greatly reduce the number of samples needed in biocompatibility studies by ensuring at the same time that all tests are done under the same conditions.
- Increase in roughness was induced by SMAT trends to improve the cellular adhesion.
- Comparatively, this increase in roughness dud not modify the proliferation capability of the cells.
- The microstructure refinement and the presence of structural defects induced by severe plastic deformation have an effect on cell distribution during the first stages of proliferation.
- Chemistry modifications are the most important factor to ensure long-term cell proliferation.
- Niobium has better long-term biocompatibility than molybdenum when it is pure or when it is alloyed with titanium.

Author Contributions: Results analysis and paper writing; L.W. and T.G.; samples preparation and biological tests, Y.N.; microscopy, M.N.; FGMs analysis, P.L.

Funding: This study was supported by the French State through the program "Investment in the Future" operated by the National Research Agency (ANR), referenced by ANR-11-LABX-0008-01 (Labex DAMAS).

Acknowledgments: The authors gratefully acknowledge the Labex Damas for its financial support, Catherine Schneider-Maunoury from Irepa Laser for the production of FGM and Natalia De Isla from Imopa laboratory in Nancy (France) for the supervision of biological tests.

Conflicts of Interest: The authors declare no conflicts of interest.

References

1. Asri, R.I.M.; Harun, W.S.W.; Samykano, M.; Lah, N.A.C.; Ghani, S.A.C.; Tarlochan, F.; Raza, M.R. Corrosion and surface modification on biocompatible metals: A review. *Mater. Sci. Eng. C* **2017**, *77*, 1261–1274. [CrossRef] [PubMed]
2. Bagherifard, S.; Ghelichi, R.; Khademhosseini, A.; Guagliano, M. Cell Response to Nanocrystallized Metallic Substrates Obtained through Severe Plastic Deformation. *ACS Appl. Mater. Interface* **2014**, *6*, 7963–7985. [CrossRef] [PubMed]
3. Kim, T.N.; Balakrishnan, A.; Lee, B.C.; Kim, W.S.; Smetana, K.; Park, J.K.; Panigrahi, B.B. In vitro biocompatibility of equal channel angular processed (ECAP) titanium. *Biomed. Mater.* **2007**, *2*, S117–S120. [CrossRef] [PubMed]
4. Kim, T.N.; Balakrishnan, A.; Lee, B.C.; Kim, W.S.; Dvorankova, B.; Smetana, K.; Park, J.K.; Panigrahi, B.B. In vitro fibroblast response to ultra fine grained titanium produced by a severe plastic deformation process. *J. Mater. Sci. Mater. Med.* **2008**, *19*, 553–557. [CrossRef] [PubMed]
5. Valiev, R.; Semenova, I.P.; Jakushina, E.; Latysh, V.V.; Rack, H.J.; Lowe, T.C.; Petruželka, J.; Dluhoš, L.; Hrušák, D.; Sochová, J. Nanostructured SPD Processed Titanium for Medical Implants. *Mater. Sci. Forum* **2008**, *584*, 49–54. [CrossRef]
6. Estrin, Y.; Ivanova, E.P.; Michalska, A.; Truong, V.K.; Lapovok, R.; Boyd, R. Accelerated stem cell attachment to ultrafine grained titanium. *Acta Biomater.* **2011**, *7*, 900–906. [CrossRef]
7. Zheng, C.Y.; Nie, F.L.; Zheng, Y.F.; Cheng, Y.; Wei, S.C.; Valiev, R.Z. Enhanced in vitro biocompatibility of ultrafine-grained titanium with hierarchical porous surface. *Appl. Surf. Sci.* **2011**, *257*, 5634–5640. [CrossRef]
8. Park, J.W.; Kim, Y.J.; Park, C.H.; Lee, D.H.; Ko, Y.G.; Jang, J.H.; Lee, C.S. Enhanced osteoblast response to an equal channel angular pressing-processed pure titanium substrate with microrough surface topography. *Acta Biomater.* **2009**, *5*, 3272–3280. [CrossRef]
9. Edalati, K.; Horita, Z. A review on high-pressure torsion (HPT) from 1935 to 1988. *Mater. Sci. Eng. A* **2016**, *652*, 325–352. [CrossRef]

10. Nie, F.L.; Zheng, Y.F.; Cheng, Y.; Wei, S.C.; Valiev, R.Z. In vitro corrosion and cytotoxicity on microcrystalline, nanocrystalline and amorphous NiTi alloy fabricated by high pressure torsion. *Mater. Lett.* **2010**, *64*, 983–986. [CrossRef]
11. Faghihi, S.; Azari, F.; Zhilyaev, A.; Szpunar, J.; Vali, H.; Tabrizian, M. Cellular and molecular interactions between MC3T3-E1 pre-osteoblasts and nanostructured titanium produced by high-pressure torsion. *Biomaterials* **2007**, *28*, 3887–3895. [CrossRef] [PubMed]
12. Korotin, D.M.; Bartkowski, S.; Kurmaev, E.Z.; Neumann, M.; Yakushina, E.B.; Valiev, R.Z.; Cholakh, S.O. Surface Studies of Coarse-Grained and Nanostructured Titanium Implants. *J. Nanosci. Nanotechnol.* **2012**, *12*, 8567–8572. [CrossRef] [PubMed]
13. Lu, J.; Zhang, Y.; Huo, W.; Zhang, W.; Zhao, Y.; Zhang, Y. Electrochemical corrosion characteristics and biocompatibility of nanostructured titanium for implants. *Appl. Surf. Sci.* **2018**, *434*, 63–72. [CrossRef]
14. Bahl, S.; Aleti, B.T.; Suwas, S.; Chatterjee, K. Surface nanostructuring of titanium imparts multifunctional properties for orthopedic and cardiovascular applications. *Mater. Des.* **2018**, *144*, 169–181. [CrossRef]
15. Nie, F.L.; Wang, S.G.; Wang, Y.B.; Wei, S.C.; Zheng, Y.F. Comparative study on corrosion resistance and in vitro biocompatibility of bulk nanocrystalline and microcrystalline biomedical 304 stainless steel. *Dent. Mater.* **2011**, *27*, 677–683. [CrossRef]
16. Zhao, M.; Wang, Q.; Lai, W.; Zhao, X.; Shen, H.; Nie, F.; Zheng, Y.; Wei, S.; Ji, J. In vitro bioactivity and biocompatibility evaluation of bulk nanostructured titanium in osteoblast-like cells by quantitative proteomic analysis. *J. Mater. Chem. B* **2013**, *1*, 1926. [CrossRef]
17. Zhang, Y.S.; Zhang, L.C.; Niu, H.Z.; Bai, X.F.; Yu, S.; Ma, X.Q.; Yu, Z.T. Deformation twinning and localized amorphization in nanocrystalline tantalum induced by sliding friction. *Mater. Lett.* **2014**, *127*, 4–7. [CrossRef]
18. Lu, K.; Lu, J. Nanostructured surface layer on metallic materials induced by surface mechanical attrition treatment. *Mater. Sci. Eng. A* **2004**, *375–377*, 38–45. [CrossRef]
19. Shot Peening for Medical Indusrty. Available online: https://sonats-et.com/en/our-markets/shot-peening-medical-industry/ (accessed on 12 December 2019).
20. Bagheri, S.; Guagliano, M. Review of shot peening processes to obtain nanocrystalline surfaces in metal alloys. *Surf. Eng.* **2009**, *25*, 3–14. [CrossRef]
21. Grosdidier, T.; Novelli, M. Recent Developments in the Application of Surface Mechanical Attrition Treatments for Improved Gradient Structures: Processing Parameters and Surface Reactivity. *Mater. Trans.* **2019**, *60*, 1344–1355. [CrossRef]
22. Arifvianto, B.; Suyitno; Mahardika, M.; Dewo, P.; Iswanto, P.T.; Salim, U.A. Effect of surface mechanical attrition treatment (SMAT) on microhardness, surface roughness and wettability of AISI 316L. *Mater. Chem. Phys.* **2011**, *125*, 418–426. [CrossRef]
23. Lai, M.; Cai, K.; Hu, Y.; Yang, X.; Liu, Q. Regulation of the behaviors of mesenchymal stem cells by surface nanostructured titanium. *Colloids Surf. B Biointerfaces* **2012**, *97*, 211–220. [CrossRef] [PubMed]
24. Zhao, C.; Ji, W.; Han, P.; Zhang, J.; Jiang, Y.; Zhang, X. In vitro and in vivo mineralization and osseointegration of nanostructured Ti6Al4V. *J. Nanoparticle Res.* **2011**, *13*, 645–654. [CrossRef]
25. Koizumi, M. FGM activities in Japan. *Compos. Part. B Eng.* **1997**, *28*, 1–4. [CrossRef]
26. Pei, E.; Loh, G.H.; Harrison, D.; de Amorim, H.A.; Monzón Verona, M.D.; Paz, R. A study of 4D printing and functionally graded additive manufacturing. *Assem. Autom.* **2017**, *37*, 147–153. [CrossRef]
27. Roop Kumar, R.; Wang, M. Functionally graded bioactive coatings of hydroxyapatite/titanium oxide composite system. *Mater. Lett.* **2002**, *55*, 133–137. [CrossRef]
28. Bogdanski, D.; Köller, M.; Müller, D.; Muhr, G.; Bram, M.; Buchkremer, H.P.; Stöver, D.; Choi, J.; Epple, M. Easy assessment of the biocompatibility of Ni–Ti alloys by in vitro cell culture experiments on a functionally graded Ni–NiTi–Ti material. *Biomaterials* **2002**, *23*, 4549–4555. [CrossRef]
29. Qian, T.; Liu, D.; Tian, X.; Liu, C.; Wang, H. Microstructure of TA2/TA15 graded structural material by laser additive manufacturing process. *Trans. Nonferrous Met. Soc. China* **2014**, *24*, 2729–2736. [CrossRef]
30. Ren, H.S.; Liu, D.; Tang, H.B.; Tian, X.J.; Zhu, Y.Y.; Wang, H.M. Microstructure and mechanical properties of a graded structural material. *Mater. Sci. Eng. A* **2014**, *611*, 362–369. [CrossRef]

31. Naebe, M.; Shirvanimoghaddam, K. Functionally graded materials: A review of fabrication and properties. *Appl. Mater. Today* **2016**, *5*, 223–245. [CrossRef]
32. Bartakova, S.; Prachar, P.; Kudrman, J.; Bresina, V.; Podhorna, B.; Cernochova, P.; Vanek, J.; Strecha, J. New titanuim β-alloys for dental implantology and their laboratory-based assays of biocompatibility. *Scr. Med.* **2009**, *82*, 76–82.
33. Cremasco, A.; Messias, A.D.; Esposito, A.R.; de Rezende Duek, E.A.; Caram, R. Effects of alloying elements on the cytotoxic response of titanium alloys. *Mater. Sci. Eng. C* **2011**, *31*, 833–839. [CrossRef]
34. Schneider-Maunoury, C.; Weiss, L.; Perroud, O.; Joguet, D.; Boisselier, D.; Laheurte, P. An application of differential injection to fabricate functionally graded Ti-Nb alloys using DED-CLAD®process. *J. Mater. Process. Technol.* **2019**, *268*, 171–180. [CrossRef]
35. Schneider-Maunoury, C.; Weiss, L.; Acquier, P.; Boisselier, D.; Laheurte, P. Functionally graded Ti6Al4V-Mo alloy manufactured with DED-CLAD®process. *Addit. Manuf.* **2017**, *17*, 55–66. [CrossRef]
36. Novelli, M.; Bocher, P.; Grosdidier, T. Effect of cryogenic temperatures and processing parameters on gradient-structure of a stainless steel treated by ultrasonic surface mechanical attrition treatment. *Mater. Charact.* **2018**, *139*, 197–207. [CrossRef]
37. Samih, Y.; Novelli, M.; Thiriet, T.; Bolle, B.; Allain, N.; Fundenberger, J.J.; Marcos, G.; Czerwiec, T.; Grosdidier, T. Plastic deformation to enhance plasma-assisted nitriding: On surface contamination induced by Surface Mechanical Attrition Treatment. *IOP Conf. Ser. Mater. Sci. Eng.* **2014**, *63*, 012020. [CrossRef]
38. Alikhani Chamgordani, S.; Miresmaeili, R.; Aliofkhazraei, M. Improvement in tribological behavior of commercial pure titanium (CP-Ti) by surface mechanical attrition treatment (SMAT). *Tribol. Int.* **2018**, *119*, 744–752. [CrossRef]
39. Wen, L.; Wang, Y.; Zhou, Y.; Guo, L.X.; Ouyang, J.H. Iron-rich layer introduced by SMAT and its effect on corrosion resistance and wear behavior of 2024 Al alloy. *Mater. Chem. Phys.* **2011**, *126*, 301–309. [CrossRef]
40. Wen, L.; Wang, Y.; Jin, Y.; Ren, X. Comparison of corrosion behaviour of nanocrystalline 2024-T4 Al alloy processed by surface mechanical attrition treatment with two different mediums. *Corros. Eng. Sci. Technol.* **2015**, *50*, 425–432. [CrossRef]
41. Zheng, Y.; Zeng, W.; Wang, Y.; Zhang, S. Kink deformation in a beta titanium alloy at high strain rate. *Mater. Sci. Eng. A* **2017**, *702*, 218–224. [CrossRef]
42. Lee, C.M.; Ju, C.P.; Chern Lin, J.H. Structure-property relationship of cast Ti-Nb alloys. *J. Oral Rehabil.* **2002**, *29*, 314–322. [CrossRef] [PubMed]
43. Thoemmes, A.; Bataev, I.A.; Belousova, N.S.; Lazurenko, D.V. Microstructure and mechanical properties of binary Ti-Nb alloys for application in medicine. In Proceedings of the 2016 11th International Forum on Strategic Technology (IFOST), Novosibirsk, Russia, 1–3 June 2016; pp. 26–29.
44. Ho, W.F. Effect of omega phase on mechanical properties of Ti-Mo alloys for biomediacal applications. *J. Med. Biol. Eng.* **2007**, *28*, 47–51.
45. Sadeghpour, S.; Abbasi, S.M.; Morakabati, M.; Karjalainen, L.P. Effect of dislocation channeling and kink band formation on enhanced tensile properties of a new beta Ti alloy. *J. Alloys Compd.* **2019**, *808*, 151741. [CrossRef]
46. Deligianni, D.D.; Katsala, N.; Ladas, S.; Sotiropoulou, D.; Amedee, J.; Missirlis, Y.F. Effect of surface roughness of the titanium alloy Ti}6Al}4V on human bone marrow cell response and on protein adsorption. *Biomaterials* **2001**, *22*, 1241–1251. [CrossRef]
47. Huang, H.H.; Ho, C.T.; Lee, T.H.; Lee, T.L.; Liao, K.K.; Chen, F.L. Effect of surface roughness of ground titanium on initial cell adhesion. *Biomol. Eng.* **2004**, *21*, 93–97. [CrossRef]
48. Rosales-Leal, J.I.; Rodríguez-Valverde, M.A.; Mazzaglia, G.; Ramón-Torregrosa, P.J.; Díaz-Rodríguez, L.; García-Martínez, O.; Vallecillo-Capilla, M.; Ruiz, C.; Cabrerizo-Vílchez, M.A. Effect of roughness, wettability and morphology of engineered titanium surfaces on osteoblast-like cell adhesion. *Colloids Surf. Physicochem. Eng. Asp.* **2010**, *365*, 222–229. [CrossRef]
49. Johansson, C.B.; Albrektsson, T.; Ericson, L.E.; Thomsen, P. A quantitative comparison of the cell response to commercially pure titanium and Ti-6Al-4V implants in the abdominal wall of rats. *J. Mater. Sci. Mater. Med.* **1992**, *3*, 126–136. [CrossRef]

50. Eisenbarth, E.; Velten, D.; Müller, M.; Thull, R.; Breme, J. Biocompatibility of β-stabilizing elements of titanium alloys. *Biomaterials* **2004**, *25*, 5705–5713. [CrossRef]
51. Ju, C.P.; Lee, C.M.; Chern Lin, J.H. Medical Implant Made of Biocompatible Low Modulus High Strength Titanium-Niobium Alloy and Method of Using the Same. Patent US20020162608A1, 7 November 2002.